IEEE Access
Multidisciplinary | Rapid Review | Open Access Journal

IEEE ENGINEERING IN MEDICINE AND BIOLOGY SOCIETY SECTION

Received 13 February 2023, accepted 12 March 2023, date of publication 23 March 2023, date of current version 29 March 2023.

Digital Object Identifier 10.1109/ACCESS.2023.3260982

RESEARCH ARTICLE

Multiple Sclerosis Disease Evolution Assessment in Brain MRI Lesions Based on Texture and Multi-Scale Amplitude Modulation-Frequency Modulation (AM-FM) Features

CHRISTOS P. LOIZOU[1], (Senior Member, IEEE), KEVIN FOTSO[2], (Member, IEEE), ANTRIA NICOLAOU[3,4], (Member, IEEE), MARIOS PANTZARIS[5], MARIOS S. PATTICHIS[2,6], (Senior Member, IEEE), AND CONSTANTINOS S. PATTICHIS[3,4,7], (Fellow, IEEE)

[1]Department of Electrical Engineering, Computer Engineering and Informatics, Cyprus University of Technology, 3036 Limassol, Cyprus
[2]Department of Biomedical Engineering, The University of New Mexico, Albuquerque, NM 87131, USA
[3]Department of Computer Science, University of Cyprus, 1678 Nicosia, Cyprus
[4]Biomedical Engineering Research Centre, University of Cyprus, 1678 Nicosia, Cyprus
[5]Cyprus School of Molecular Medicine, The Cyprus Institute of Neurology and Genetics, 1683 Nicosia, Cyprus
[6]Department of Electrical and Computer Engineering, The University of New Mexico, Albuquerque, NM 87131, USA
[7]CYENS—Centre of Excellence, 1016 Nicosia, Cyprus

Corresponding author: Christos P. Loizou (christos.loizou@cut.ac.cy)

This work was supported in part by the European Union's Horizon 2020 Research and Innovation Program under Grant 739578; and in part by the Government of the Republic of Cyprus through the Deputy Ministry of Research, Innovation and Digital Policy.

ABSTRACT Monitoring disease evolution in Multiple sclerosis (MS) subjects may aid in decision making for personalizing treatment and disease evolution prediction. We investigate the use of disability progression, using clinical features, the expanded disability status scale (EDSS), and their relationship with texture features and Amplitude Modulation-Frequency Modulation (AM-FM) features extracted from MRI MS detectable lesions for the prognosis of future disability on magnetic resonance imaging (MRI). MS detectable brain lesions from N=38 symptomatic untreated subjects diagnosed with clinically isolated syndrome (CIS), were manually segmented, by an experienced MS neurologist, on transverse T2-weighted (T_2W) images obtained from serial brain MRI scans at the baseline ($Time_{0M}$) and the repeat ($Time_{6-12M}$) examinations. The subjects were separated into two different groups based on their EDSS: (G_1: $1 \leq EDSS_{2Y} \leq 3.5$ (N=26) and G_2: $3.5 < EDSS_{2Y} \leq 8.5$ (N=12) and were monitored over ten years' time ($Time_{10Y}$). After intensity normalization and image registration, texture and AM-FM features were extracted from all MS lesions at $Time_{0M}$ and $Time_{6-12M}$. The extracted features were used to develop models that correlated with the disease progression in $Time_{10Y}$. We found statistically significant differences for features extracted from the two different groups (G_1 vs G_2 at $Time_{10Y}$) and these might be used to predict the development and or the severity of the MS disease. The best model for classifying G_1 vs G_2 subjects at $Time_{10Y}$ included information taken from the MS lesion images, texture features and AM-FM features extracted from those MS lesion images (with a correct classification score of %CC=94). The proposed methodology may contribute to additional factors for predicting the development and assessing the severity of the MS disease. However, a larger scale study is needed to establish the application in clinical practice and for computing additional features that may provide information for better and earlier differentiation between normal tissue and MS lesions.

INDEX TERMS MRI, multiple sclerosis, disease evolution, EDSS, texture analysis, AM-FM analysis, classification analysis.

The associate editor coordinating the review of this manuscript and approving it for publication was Alessandra Bertoldo.

NOMENCLATURE

The following abbreviations were used in this study:

AM-FM:	Amplitude Modulation-Frequency Modulation.
ASM:	Angular second moment.
AUC:	Area under the ROC curve.
CDF:	Cumulative distribution function.
CIS:	Clinical Isolated Syndrome.
CSF:	Cerebrovascular fluid.
%CC:	Percentage of correct classifications score.
DE:	Difference entropy.
DV:	Difference variance.
$EDSS_{2Y}$:	Expanded disability status scale at year 2.
$EDSS_{5Y}$:	Expanded disability status scale at year 5.
$EDSS_{10Y}$:	Expanded disability status scale at year 10.
FDTA:	Fractal dimension texture analysis.
FPS:	Fourier power spectrum.
G_1, G_2:	Two different groups of subjects investigated.
GLD:	Gray level distribution.
GLDS:	Gray level statistics.
IA:	Instantaneous amplitude.
IP:	Instantaneous phase.
IDM:	Inverse difference moment.
IF:	Instantaneous frequency.
|IF|:	IF magnitude.
IMC:	Information measures of correlation.
IQR:	Interquartile range.
LRE:	Long run emphasis.
LTEM:	Laws texture energy measures.
MAE:	Mean absolute error.
MRI:	Magnetic resonance image.
MS:	Multiple sclerosis.
N:	Number of cases investigated.
NAWM:	Normal appearing white matter at Time0M.
NGTDM:	Neighborhood gray tone difference matrix.
NS:	Non-statistically significant different.
NWM:	Normal white matter.
PLD:	Run length distribution.
RAE:	Relative absolute error.
RBF:	Gaussian radial basis function.
RMSE:	Root mean squared error.
ROC:	Receiver operating characteristics.
ROI:	Region of interest.
RP:	Run percentage.
RRSE:	Root relative squared error.
RUN:	Gray level run length statistics.
S:	Statistically significant difference.
SA:	Sum average.
SE:	Sum entropy.
SF:	Statistical features.
SFM:	Statistical feature matrix.
SGLDM:	Spatial gray level dependence matrices.
SGLDS:	Gray level difference statistics.
SOSV:	Sum of squares variance.
SP:	Shape parameters.
SRE:	Short run emphasis.
SV:	Sum variance.
SVM:	Support vector machines.
T_{2W}:	T_2 weighted MR images.
$Time_{0M}$:	Examination at baseline (initial examination).
$Time_{5Y}$:	Examination at 5 years after $Time_0$.
$Time_{10Y}$:	Examination at 10 years after $Time_0$.
$Time_{6-12M}$:	Examination at follow-up scan after 6-12 months.
TP / FP:	True positives / false positives.

I. INTRODUCTION

Multiple Sclerosis (MS) is a potentially disabling disease of the central nervous system (brain and spinal cord) [1]. In MS, the immune system attacks the protective sheath (myelin) that covers nerve fibers and causes communication problems between the brain and the rest of the body. MS can cause permanent damage or deterioration of the nerves, including inflammation, demyelination, axonal degeneration, and neuronal loss [1]. The EDSS assessment scores may vary among clinicians, particularly regarding the development of disability [2], [3]. A specialized neurologist's evaluation of MS is often based on clinical signs and symptoms, conventional magnetic resonance imaging (MRI), and the McDonald criteria, which were first proposed in [4] and modified in [5] and [6]. Changes in disability are strongly correlated with the development of new brain MS lesions [3]. Disability progression in MS is mediated by acute inflammation as well as chronic inflammation and neurodegeneration [3], [4], [5], [6], [7], [8]. The clinical disability is assessed at the time of each scan, using the McDonald Expanded Disability Status Scale (EDSS) [4], [5], [6], [7]. It was shown that brain and focal lesion volume measures, magnetization transfer ratio and texture features extracted from the MS lesions can provide new information in diagnosing MS [8], [9]. Texture [9] and Amplitude Modulation-Frequency-Modulation (AM-FM) features [10] characterize MRI MS lesions and also the macroscopic abnormalities that may be unnoticeable using conventional measures of lesion volume and number [11]. The motivation of this study was to investigate the usefulness of texture and AM-FM feature analysis for following up MS disease evolution.

It was shown in [12] that baseline MRI findings maybe predictive for development of clinically definite MS using the lesion volume and that its change at earlier time can be correlated with disability. More specifically, it was shown in [12], that the EDSS correlated moderately with lesion volume in MRI at 5 years ($\rho = 0.60$), and with an increase of lesion volume over the first 5 years of the MS disease ($\rho = 0.61$) [13]. It was also shown in [14] that higher EDSS correlates with lower volumes of brain, grey and white matter, and some subcortical structures, but also with higher T_2 lesion load.

TABLE 1. Median (IQR) demographics and EDSS groups of the study (N=38). EDSS score at year 10 was used for studying MS disease evolution.

	All	G_1 0.0≤EDSS≤3.5	G_2 3.5<EDSS≤10.0	G_1 vs G_2	No. of MS lesions
N ($Time_{2Y}$/$Time_{5Y}$/ $Time_{10Y}$)	38 / 38 / 38	37 / 29 / 26	1 / 9 / 12		
Sex (F/M) ($Time_{2Y}$/$Time_{5Y}$/ $Time_{10Y}$)	(21/17) / (21/17) / (22/16)	(36/1)/(17/12)/(15/11)	(1/-) /(4/5)/(5/7)		
Age_{2Y}	30(11.5)	21(10)	22(15)		222
Age_{5Y}	33(11.5)	23(11)	26(16)		289
Age_{10Y}	38(11.5)	25(13)	30(19)		327
$EDSS_{2Y}$	2.0(1.0)	2.0(0.9)	2.8(0.5)	S (p=0.0003)	
$EDSS_{5Y}$	2.5(1.0)	2.0(0.9)	4.5(1.3)	S (p=0.0001)	
$EDSS_{10Y}$	3.0(2.3)	3.0(0.5)	5.8(1.5)	S (p=0.0001)	

N: Number of MS patients: F: Female; M: Male; IQR: Inter-Quartile Range; $EDSS_{2Y}$, $EDSS_{5Y}$, $EDSS_{10Y}$: EDSS at $Time_{2Y}$, $Time_{5Y}$ and $Time_{10Y}$ respectively; S: Statistical significance difference at p<0.001 for the Mann-Whitney rank sum test.

In another study [15], it was shown that radiomics texture analysis may be used to predict normal appearing white matter (NAWM), which will evolve into MS lesions. In [16], texture analysis has been applied in cross-sectional studies of patients with small vessel diseases. It was shown that radiomics may be used to investigate the microstructural changes of NAWM. It was also recently documented in [17] that the high number of relapses can be used as an early marker for identifying patients worsening in the presence of MS activity. Finally, in [18] the disability evolution in MS patients was predicted using a latent class linear mixed model with an accuracy of 94%. Demographic, clinical and imaging variables were used for the classification.

Other studies have discussed how texture features can be used for the assessment of MS lesions in: (i) differentiating between lesions for normal white matter (NWM), and the so called NAWM, and (ii) monitoring the progression of the disease over longitudinal scans [8], [9], [10], [11], [19], [20], [21], [22], [23], [24], [25], [26], which is the objective of this paper as well. In [26] the performance of texture analysis concerning discrimination between MS lesions, NAWM and NWM from healthy controls was investigated by using linear discriminant analysis. The results suggested that texture features can support early diagnosis in MS.

Our primary objective in this study was to investigate whether disease evolution in MS subjects maybe predicted using the EDSS, and its relationship with texture and AM-FM features extracted from MRI MS detectable lesions at the baseline examination. This will aid in decision making in the prognosis of future disability for personalizing treatment and disease evolution prediction. Since the use of quantitative MRI analysis as a surrogate outcome is also used as a replacement measure in clinical trials, we hypothesize that there is a close relationship between the change in the extracted features and the clinical status and the rate of development of disability. We analyzed subject's images acquired at the initial ($Time_{0M}$) and repeat ($Time_{6-12M}$) examinations and we correlated texture and AM-FM feature findings with disability assessment scales. We analyze how the EDSS scores relate with standard shape, texture, AM-FM and other image features.

In comparison to previous studies, the current paper makes three distinct contributions. First, the current paper is focused on a new application. The current application is focused on the early detection of AM-FM features that can be used to predict significant advancement in the EDSS scores. Second, the paper introduces a new set of AM-FM features. We introduce the use of the cumulative distribution functions (CDF) of the instantaneous frequency (IF) at different scales. Third, the paper uses a new Gabor filterbank that was first introduced in [27].

The layout of the paper is as follows: Section II presents the materials and methods, while section III presents the results of the study. Finally, Section IV presents the discussion, the limitations of the study and the future work.

II. MATERIALS AND METHODS

The system diagram presented in Fig. 1 illustrates the process followed in the MRI NAWM and lesion analysis performed in this study. The different processing steps for the analysis of the extracted ROIs are analyzed herein below.

To introduce the objective of our study, an example in Fig. 2 is presented. Here, we show two transaxial T_{2W} MR images acquired from a subject with an EDSS≤3.5 in a) and a subject with an EDSS>3.5 in Fig. 2b). Segmented MS lesions are shown with outlines for both subjects.

A. STUDY GROUP AND MRI ACQUISITION

The characteristics of the group investigated in this study are summarized in Table 1. All subjects with a suggestive clinical isolated syndrome (CIS) and MRI-detectable brain lesions were scanned at baseline ($Time_{0M}$) and with an interval of 6-12 months ($Time_{6-12M}$). The transverse MR images used for analysis were obtained using a T_{2W} turbo spin echo pulse sequence (repetition time = 4408 ms, echo time = 100 ms, echo spacing = 10.8 ms). The reconstructed image had a slice thickness of 5 mm and a field of view of 230 mm with a pixel resolution of 2.226 pixels per mm. Standardized planning procedures were applied during each MRI examination. The MR images were acquired using a 1.5T whole body Philips ACS NT MR imager (Philips Medical Systems, Best, the Netherlands). A built-in quadrature radiofrequency body coil and a quadrature radio frequency head coil were used for proton excitation and signal detection respectively. The MRI protocol and the acquisition parameters were also given in detail in [9] and [10]. It is noted that CIS is a single episode

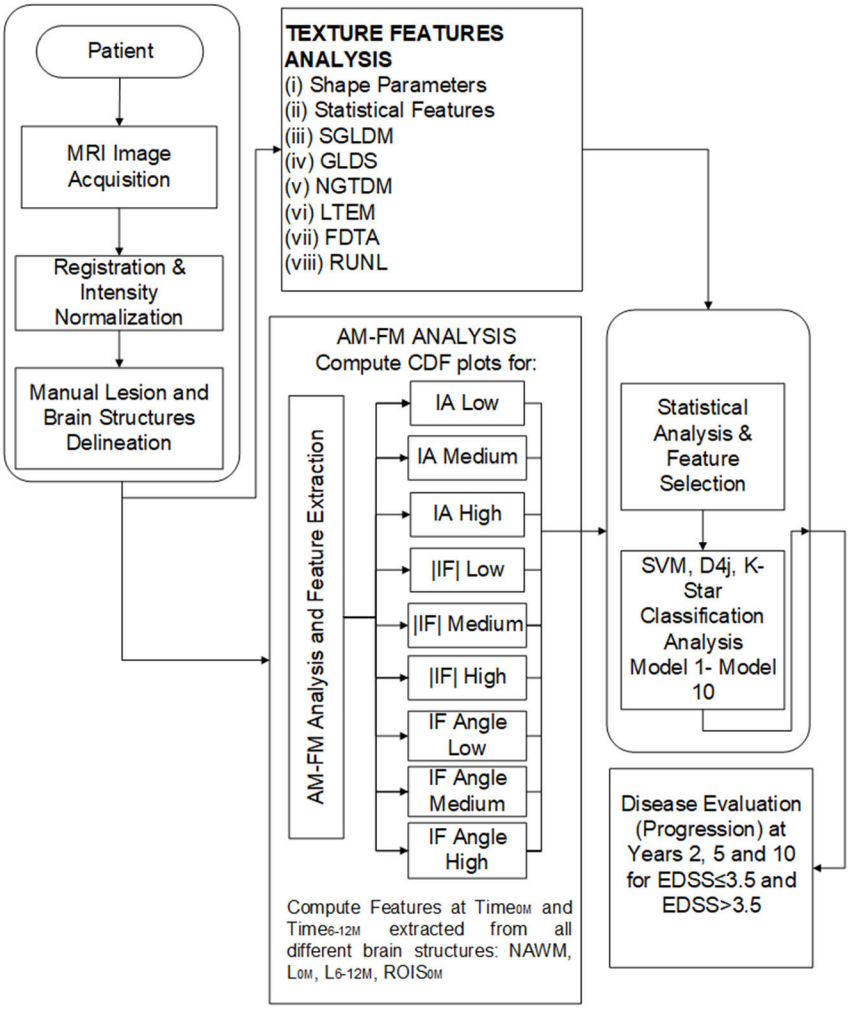

FIGURE 1. MRI image analysis system diagram for MS disease evolution assessment. MRI: Magnetic Resonance Imaging. EDSS score at year 10 was used for studying MS disease evolution in this study.

of neurological symptoms that need treatment with various outcomes depending on the severity of symptoms and the residual symptoms after treatment. The repeat MRI scans at $\text{Time}_{6-12\text{M}}$ were not related to the outcome of the CIS but rather to depicting new T_{2W} lesions which were correlated with an increased probability of transformation of CIS to clinically definite MS. The mean time difference between $\text{Time}_{0\text{M}}$ and $\text{Time}_{6-12\text{M}}$MRI examinations was about 8.5 months. The investigation and follow-up were based on the analysis of T_2 lesions from MRI images. This imaging has always been used in clinical and MRI studies in MS and also for the assessment of the MS MacDonald's MRI diagnostic criteria [4], [5], [6], [7].

Initial clinical evaluation was made by an experienced MS neurologist (co-author, M. Pantzaris) who referred the 38 subjects for a baseline MRI ($\text{Time}_{0\text{M}}$), upon diagnosis and clinically followed all subjects for over ten years. All subjects remained untreated between $\text{Time}_{0\text{M}}$ and $\text{Time}_{6-12\text{M}}$. At $\text{Time}_{0\text{M}}$ the stage of the disease was evaluated using the EDSS score [4], [5], [6], [7]. All subjects were also examined two years after initial diagnosis to quantify disability [4], [5], [6], [7] ($\text{EDSS}_{2\text{Y}}$), and then again in five ($\text{EDSS}_{5\text{Y}}$), and ten ($\text{EDSS}_{10\text{Y}}$), years. The subjects were also separated into two different EDSS groups (i.e. G_1: EDSS$\leq$3.5 and G_2: EDSS$>$3.5), (see also Table 1 and Fig. 3). Figure 3 illustrates box plots for the two EDSS groups distribution at years two, five and ten. The reason for selecting an EDSS cutoff point of 3.5 is that for an EDSS$>$3.5 the physician can assess neurological signs, meaning that the subject starts showing signs of disability progression. As a result, any subject having an EDSS$\leq$3.5 at two, five and ten years after the initial MRI scan can be regarded as having a rather benign course of the disease. It is known that the initial (presenting) EDSS is not strongly associated with future disability [4], [5], [6], [7]. It is noted that EDSS at baseline ($\text{Time}_{0\text{M}}$), was not used since our study focuses on texture analysis of T_2 brain MRI

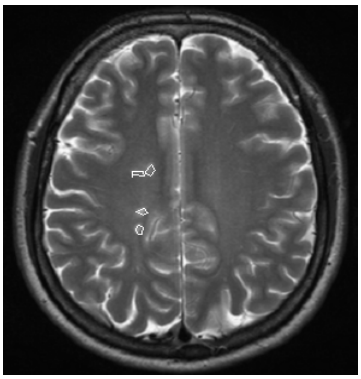

a) MRI image of the brain from a patient with $EDSS_{10Y} \leq 3.5$

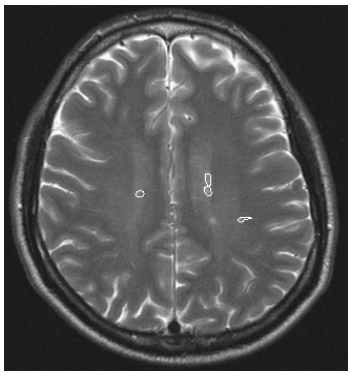

b) MRI image of the brain from a patient with $EDSS_{10Y} > 3.5$

FIGURE 2. ROIs drawn on MR image of the brain at $Time_{0Y}$, obtained from: a) a 42-year-old female MS patient with an EDSS 2.0/2.5/3.0 and b) a 45-year-old male subject with an EDSS 2.5/4.5/7.5 (measured in $Time_{2Y}$ -/, $Time_{5Y}$ /-/ and $Time_{10Y}$ /- after the initial examination). Segmented MS lesions are shown with outlines for both patients, acquired at a pixel resolution of 2.226 pixels per mm. The average gray scale median of all lesions was 91±12 and 140±14 (max=255) for the images in a) and b) respectively.

scans and future disability progression, as measured at two and five years after the initial ($Time_{0M}$) MRI scan. Additional acquisition parameters used in this study may also be found in [7], [9], and [10].

Additionally, brain imaging from 20 healthy, age-matched (mean ± SD: 30.8 ± 7.6) volunteers (8 males, and 12 females) were carried out to allow segmentation and analysis of brain NWM as it was also documented in [9] and [10].

B. REGISTRATION AND INTERSCAN INTENSITY NORMALIZATION

$Time_{6-12M}$MRI images were registered to $Time_{0M}$ images using the method introduced in [28] and used in [29], and the registration process was also applied to the lesion masks. For the registration, 6 degrees-of-freedom were used to provide rigid body transformation between the $Time_{0M}$ and $Time_{6-12M}$.

All images used in this work were intensity normalized as introduced in [28] and documented in [9] and [10] where all additional details about the algorithm may be found. A normalization algorithm adjusted distributions of each follow-up scan ($Time_{6-12M}$), to match those of the chosen baseline ($Time_{0M}$) scan in order to improve image visibility, reduce

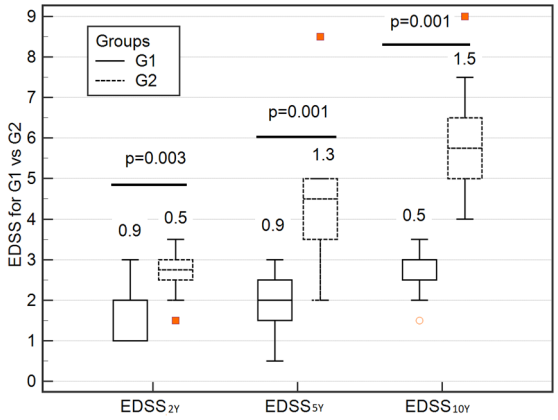

FIGURE 3. Box plots for the EDSS distribution at years two ($EDSS_{2Y}$), five ($EDSS_{5Y}$), and ten ($EDSS_{10Y}$), for two different groups (G_1: EDSS≤3.5, full line plots) vs G_2: EDSS>3.5, dotted line plots). EDSS score at year 10 was used for studying MS disease evolution in this study.

partial volume effects and facilitate MR image comparability between serial MR scans [23], such as those obtained from the MS group of this work. For the purpose of intensity normalization, the neurologist manually segmented cerebrovascular fluid (CSF) areas as well as areas with air (sinuses) from all MS brain scans as will be described in the next subsection.

C. MANUAL DELINEATION OF LESIONS, REGIONS OF INTEREST, AND NAWM

All MRI-detectable brain lesions were identified and segmented by an experienced MS neurologist and confirmed by a radiologist (see also Fig. 2). Only well-defined areas of hyper intensity on T_{2W} MR images were considered as MS plaques. The neurologist manually delineated the brain lesions by selecting consecutive points at the visually defined borders between the lesions and the adjacent NAWM on the acquired transverse T_{2W} sections. The manual delineations were performed using a graphical user inter-face implemented in Matlab® developed by our group. Every effort was made to avoid white matter areas with subtle, patchy and diffuse abnormal signal intensities. Finally, the neurologist manually segmented cerebrovascular fluid (CSF) areas as well as areas with air (sinuses) from all MS brain scans based on the method introduced in [9]. Similarly, regions of interest (ROIs) representing NWM, CSF and air from the sinuses were segmented from 20 MRI scans acquired from healthy subjects. Manual segmentation by the MS expert was performed in a blinded manner (without knowledge of the MRI-subject time-point relationships), without the possibility of identifying the subject, the time-point of the exam or the clinical findings. The selected points and delineations were saved to be used for texture feature extraction and AM-FM analysis (see also subsections II.E and II.F).

D. ROIS IDENTIFICATION

ROIS were identified by the experienced neurologist in three steps. First, the corresponding slices between $Time_{0M}$ and $Time_{6-12M}$were registered. Second, NAWM

regions were segmented at $Time_{0M}$ and $Time_{6-12M}$($NAWM_0$, $NAWM_{6-12}$). Third, NWM and CSF regions from healthy MRI brain scans were also segmented.

E. FEATURE EXTRACTION: SHAPE AND TEXTURE

Shape features and texture features were extracted from all MS lesions detected and segmented, from the segmented ROIs, NAWM regions as well as from the brain scan of 20 healthy subjects. The overall shape and texture features for each subject were then estimated by averaging the corresponding values for all lesions for each group of subjects. The following group of features were extracted: 12 Shape Parameters (SP) [26], [29], [30], 5 Statistical Features (SF) [30], [31], 14 Spatial Gray Level Dependence Matrices (SGLDM) as proposed by Haralick et al. [31], 5 Gray Level Difference Statistics (GLDS) [32], 5 Neighborhood Gray Tone Difference Matrix (NGTDM) [33], 4 Statistical Feature Matrix (SFM) [34], 6 Laws Texture Energy Measures (LTEM) [34], 4 Fractal Dimension Texture Analysis (FDTA) and 5 Gray Level Run Length Statistics (RUNL) [35]. These features were computed using the IDF toolbox implemented in Matlab®R2015 software toolbox, where additional details may also be found in [9] and [10].

F. AM-FM ANALYSIS

AM-FM analysis extracts AM-FM features at different frequency scales. Here, we note that frequency measurements are expressed in terms of cycles per mm based on a resolution of 2.226 pixels per mm. Furthermore, frequency angle is expressed in radians and is physically meaningful due to image registration. Similarly, amplitude components are also standardized due to scan normalization. Then, over each segmented region, we compute a multiscale AM-FM decomposition using [27] (also see [36]):

$$\boldsymbol{I(x,y)} = \sum_{\boldsymbol{n=1}}^{\boldsymbol{M}} \boldsymbol{a_n}\,(x,y)\, cos\boldsymbol{\phi_n}\,(x,y)$$

where $n = 1, 2, 3$ correspond to the low, medium, and high scales, $a_n(x, y)$ denote the instantaneous amplitude (IA) components, and $\varphi_n(x, y)$ denote the instantaneous phase components. For each AM-FM component, we have the associated instantaneous frequency (IF): $\nabla\varphi_n(x, y)$ that is estimated as described in [27].

As an image representation, we note that the FM images $\cos\varphi_n(x, y)$ describe fast changing texture components. The IA components $a_n(x, y)$ can be used to quantify the contributions of each component. We extract AM-FM features for each lesion. Over each lesion, for each one of the three scales, we compute 14-bin histograms of the IA, IF angle, and IF magnitude. To differentiate among scales, we refer to each AM-FM feature by its frequency scale. Thus, low-IA, medium-IA and high-IA refer to IA components from the low, medium, and high frequency scales. For each AM-FM feature, we compute cumulative distribution functions (CDFs) at $Time_{0M}$ and $Time_{6-12M}$.

G. STATISTICAL ANALYSIS

The Mann-Whitney non-parametric rank sum test (for independent samples of different sizes) [36] was used in order to identify if there were significant differences (S) at $p<0.05$ or not (NS) at $p\geq0.05$, between the extracted texture and AM-FM features from the two different groups (G_1 vs G_2). The median values over the segmented components (NWM, NAWM, and MS lesions) were used for investigating the relationships between the texture features extracted from all brain structures between $Time_{0M}$ and $Time_{6-12M}$ intervals. Additionally, the test was performed for subjects with an EDSS$\leq$3.5 versus EDSS$>$3.5, evaluated two years after the initial MRI examination. Subjects with EDSS$\leq$3.5 were assigned the binary number 0, while subjects with EDSS$>$3.5 were assigned the binary number 1. This was carried out to investigate whether texture features extracted from the above areas of the brain may be able to distinguish between the two different EDSS groups. Similarly, for comparing independent samples from equal populations, the Wilcoxon non-parametric rank sum test was used [37]. Above statistical tests were also applied on the CDF plots generated from the AM-FM derived MS lesions to establish which feature shows statistically significant group difference (S), at $p<0.05$ or not (NS), at $p\geq0.05$.

Box plots were used to compare the texture and AM-FM features between the brain structures extracted from the two different EDSS groups. Furthermore, boxplots were used to demonstrate the difference of the grayscale values in the two different groups. Because the data were not normally distributed 1st, 2nd and 3rdquartiles were used.

The analysis was performed using the Matlab® R2015 software package and the MedCalc® software (Ostend, Belgium) version 19.0.3 for the statistical analysis. Bonferroni correction was used to adjust p-values and confidence intervals for the multiple comparisons performed in this study. This correction was applied in a leave-one-out fashion to get the most significant features.

H. CLASSIFICATION ANALYSIS

Texture classification modelling was used to predict EDSS score at year 10. Models to predict subjects with EDSS$\leq$3.5 versus those with EDSS$>$3.5 based on texture and AM-FM features, and lesion images were developed. The Weka 3.8 workbench [38], and two different classifiers were investigated. The classifier features were selected based on statistically significant differences as given by the Mann-Whitney rank sum tests between the two groups investigated in this study (G_1 vs G_2, see also Table 2 and Table 3). Only the most significant bins from the AM-FM features that showed statistical significant difference at $p<0.05$, between groups were selected (see underlined features in Table 3). The classification analysis performance metrics documented in this study were based on the evaluation set.

We investigated the Support Vector Machines (SVM) [39] classifier and the Deeplearning4j package [40].

TABLE 2. Texture features median (IQR) values for the MS lesions at time $_{0M}$ and time 6 – 12M for two different EDSS groups (g). (G1: EDSS≤3.5/ G2: EDSS>3.5) at year 10, that showed statistical significance. * mann whitney rank-sum test at P<0.05. the number of subjects in G1 and G2 were 26 and 12 respectivel.

Texture Features	Texture Features at $Time_{0M}$ and $Time_{6-12M}$ Based on Groups at Year 10			
	G_1 / G_2 at $Time_{0M}$	G_1 vs G_2^* p-value	G_1 / G_2 at $Time_{6-12M}$	G_1 vs G_2^* p-value
Spatial Gray Level Dependence Matrix ($SGLDM_m$) - Mean Values				
Correlation	0.79 (0.13) / 0.88 (0.08)	0.024	-	-
SE	4.0 (0.59) / 4.4.2 (0.39)	0.035	-	-
Entropy	5.2 (0.95) / 5.72 (0.56)	0.04	-	-
Spatial Gray Level Dependence Matrix ($SGLDM_r$) - Range of Values				
Correlation	0.22 (0.138) / 0.12 (0.09)	0.04	-	-
DE	-	-	0.412 (0.09) / 0.449 (0.1)	0.006
Neighbourhood Gray Tone Difference Matrix (NGTDM)				
Coarseness	10.69 (6.37) / 17.41 (9.15)	0.012	13.27 (9.11) / 18.79 (7.13)	0.024
Contrast	1.3 (1.93) / 0.55 (0.331)	0.02	-	-
Busyness*10^3	0.82 (0.21) / 0.21 (0.38)	0.019	-	-
Strength/10^3	19.6 (36) / 60.7 (71)	0.033	26.1 (37.94) / 56.7 (62.64)	0.014
Fractal Dimension Analysis (FDTA)				
H_1	-	-	0.45 (0.062) / 0.49 (0.046)	0.033
H_2	0.25 (0.16) / 0.33 (0.13)	0.02	0.26 (0.146) / 0.34 (0.086)	0.031
Fourier Power Spectrum (FPS)				
RS	1254 (840) / 1863 (721)	0.033	1125 (1037) / 1752 (614)	0.038
Gray Level Run Length Statistics (RUNL)				
$Runl_{SRE}$	0.89 (0.039) / 0.91 (0.04)	0.034	-	-
$Runl_{RLD}$*10^3	11.77 (14.68) / 20.44 (4.67)	0.001	12.34 (10.1) / 17.5 (9.33)	0.03
$Runl_{LRE}$	1.69 (0.94) / 2.62 (1.11)	0.009	-	-
$Runl_{RP}$	-	-	1.43 (0.72) / 2.77 (1.27)	0.02

G_1, G_2: Patient Groups with 0.0≤EDSS≤3.5 (NR=12) and 3.5>EDSS≤10.0 respectively. SE: Sum Entropy, DE: Difference entropy, H_1, H_2: Hurst coefficients, RS: Radial Sum, Runl: Gray level run length statistics for: short run emphasis (SRE), run length distribution (RLD), long run emphasis (LRE), Run percentage (RP).

TABLE 3. AM-FM median (IQR) texture features between the high if features extracted from the MS lesions at time $_{0M}$ and time $_{6-12M}$ for the two different edss groups (g_1: EDSS ≤3.5/ g_2: EDSS>3.5) at year 10, which showed statistical significance. * Mann-Whitney rank-sum test at p<0.05.

Texture Features at $Time_{0M}$ and $Time_{6-12M}$ Based on Groups at Year 10				
AM-FM CDF BinFeatures	G_1 / G_2 at $Time_{0M}$	G_1 vs G_2^* p-value	G_1 / G_2 at $Time_{6-12M}$	G_1 vs G_2^* p-value
High Scale IF Magnitude in Cycles per mm				
CDF_2: 0.21	0.000 (0.000) / 0.033 (0.082)	0.038	0.000 (0.041) / 0.049 (0.054)	0.014
CDF_3: 0.31	0.009 (0.074) / 0.129 (0.160)	0.027	0.019 (0.111) / 0.164 (0.181)	0.014
CDF_4: 0.41	0.065 (0.124) / 0.283 (0.368)	0.023	0.111 (0.139) / 0.358 (0.234)	0.014
CDF_5: 0.51	0.191(0.031) / 0.503 (0.402)	0.041	0.222 (0.229) / 0.571 (0.184)	0.006
CDF_6: 0.61	0.419 (0.424) / 0.668 (0.310)	0.060	0.404 (0.329) / 0.719 (0.095)	0.005
CDF_7: 0.72	0.636 (0.398) / 0.821 (0.260)	0.080	0.690 (0.220) / 0.854 (0.045)	0.003
CDF_8: 0.82	0.874 (0.275) / 0.914 (0.133)	0.194	0.860 (0.148) / 0.946 (0.059)	0.008
CDF_9: 0.91	0.957 (0.074) / 0.979 (0.032)	0.218	0.967 (0.069) / 0.990 (0.02)	0.035
High Scale Angle in radians				
CDF_2: 0.23	0.023 (0.091) / 0.087 (0.104)	0.033	0.050 (0.141) / 0.073 (0.082)	0.154
CDF_3: 0.34	0.943 (0.226) / 0.217 (0.127)	0.041	0.154 (0.282) / 0.186 (0.140)	0.171
CDF_4: 0.45	0.215 (0.331) / 0.341 (0.215)	0.043	0.286 (0.300) / 0.358 (0.180)	0.102
CDF_5: 0.56	0.349 (0.323) / 0.465 (0.225)	0.033	0.386 (0.298) / 0.511 (0.168)	0.034
CDF_6: 0.67	0.507 (0.299) / 0.540 (0.235)	0.130	0.532 (0.230) / 0.644 (0.223)	0.023

G_1, G_2: Patient groups with 0.0≤EDSS≤3.5 (NR=26) and 3.5>EDSS≤10.0 (NR=12) respectively.

The SVM classifier [39], is a widely used model for classification analysis and it is generally accepted that it performs well compared to many other methods when applied to brain classification [41]. The SVM maps the input space to a higher dimension via a kernel function to find a hyperplane that will result in maximal discrimination. In SVM, a kernel matrix

TABLE 4. MRI MS lesions texture, AM-FM and image classification evaluation results between the two different groups at year 10 investigated in this study for $time_{0M}$(-/) and $time_{0M}$+$time_{6-12M}$ (/-), using all features that were statistically significantly different at $p<0.05$ (see also underlined features in table iii). svm and deep learning models (see first and second part of the table) were trained and evaluated using 10-fold cross validation, and the RBF kernel with C=1 and gamma=0.01. the third part of the table shows the MRI image classification results on all lesion images at $time_{0M}$(-/) and $time_{0M}$+ $time_{6-12M}$ (/-) using deep learning.

Features	Texture	AM-FM	Lesion Images	%CC	%TP	%FP	%Pre.	%Rec.	F-Measure	AUC	MAE	RMSE
SVM Classifier on Texture & AM-FM Features												
Model 1	+			70 / 79	71 / 69	29 / 39	71 / 78	71 / 79	0.82 / 0.84	.69 / .78	0.315 / 0.367	0.456 / 0.435
Model 2		+		73 / 84	73 / 96	26 / 48	74 / 83	73 / 92	0.83 / 0.83	.71 / .78	0.412 / 0.393	0.421 / 0.4678
Model 3	+	+		82 /89	83 / 96	16 / 45	84 / 89	84 / 94	0.91 / 0.84	.83 / .87	0.316 / 0.303	0.376 / 0.387
DeepLearning4j Classifier on Texture & AM-FM Features												
Model 4	+			71 / 81	71 / 80	25 / 44	73 / 77	72 / 78	0.81 / 0.86	.81 / .86	0.367 / 0.299	0.46 / 0478
Model 5		+		74 / 84	74 / 84	24 / 38	74 / 77	75 / 96	0.83 / 0.84	.73 / 79	0.397 / 0.450	0.327 / 0.298
Model 6	+	+		86 / 91	85 / 87	15 / 58	86 / 79	85 / 96	0.92 / 0.86	.84 / .88	0.326 / 0.399	0.3532 / 0.356
K-Star Beta (B 20-Ma) Classifier on Texture Features & AM-FM Features & Lesion Images												
Model 7			+	79 / 84	79 / 86	22 / 18	80 / 87	79 / 88	0.78 / 0.88	.78 / .88	0.367 / 0.389	0.564 / 0.467
Model 8	+		+	84 / 89	83 / 86	17 / 19	83 / 88	84 / 88	0.84 / 0.89	.84 / .89	0.421 / 0.421	0.534 / 0.446
Model 9		+	+	85 / 92	85 / 90	15 / 14	89 / 91	88 / 90	0.89 / 0.91	.89 / .91	0.323 / 0.423	0.501 / 0.365
Model 10	+	+	+	91 / 94	91 / 93	9 / 11	91 / 94	90 /94	0.91 / 0.94	.90 / .94	0.392 / 0.356	0.487 / 0.478

AM-FM: Amplitude modulation-frequency modulation, %CC: Percentage of correct classifications, TP: True positives, FP: False positives, Pre.: Precision=TP/(TP+FP), Rec.: Recall=TP/(TP+FN), AUC: Area under the curve, MAE: Mean absolute error, RMSE: Root mean square error.

is used that encodes the similarities between features that can be used to achieve discrimination between classes that are not linearly separable [42]. The SVM was trained and evaluated using leave-one-out 10-fold cross-validation using Gaussian Radial Basis Function (RBF) kernel with a c=1 and γ =0.01. The classifier features were selected to have statistically significant difference based on the Wilcoxon and Mann-Whitney rank sum tests between the different classes investigated.

The Deeplearning4j [40] classifier, performs classification using deep learning and convolutional neural networks. Lesion images were initially preprocessed with the Fuzzy opponent histogram filter, the edge histogram filter, and the auto correlogram filter [38], where a significantly higher number of features was generated than the number of lesion pixels (Model 7-10, see also Table 4). The lesion image features from all subjects were divided into 10 random groups and the correct classification performance was tested trained and evaluated using 10-fold cross-validation. For each set of lesion image features the procedure was repeated 10 times and the average results were computed. For Model 7-10 we used the K-Star Beta version classifier (B 20-Ma), from the Weka 3.8 neural network toolbox [40].

The performance of the classifier models was measured using the percentage of correct classifications score (%CC) based on the correctly and incorrectly classified cases and the receiver operating characteristic (ROC) metrics: true positives (TP), false positives (FP), Precision=TP/(TP+FP), Recall=TP/(TP+FN), ROC: Area under the ROC curve (AUC), mean absolute error (MAE), root mean squared error (RMSE), relative absolute error (RAE), root relative squared error (RRSE). Models based on texture and AM-FM features and lesion images were investigated.

III. RESULTS

In Table 1 we provided a summary of the demographics and the clinical characteristics of the study population used in this work. We observe an increase in the EDSS for both groups of subjects (G_1 and G_2), with an increasing duration of the disease. There are also statistically significant differences for the EDSS scores, between the two EDSS groups both at $Time_{2Y}$ (p=0.0003), and at $Time_{10Y}$ (p=0.0001). Statistically significant differences were also found between G_1 vs G_2 for the $EDSS_{2Y}$ vs $EDSS_{10Y}$.

A. TEXTURE ANALYSIS

In Table 2 we present the texture features median (IQR) values extracted from the brain MS lesions at $Time_{0M}$ (left column of Table 2), and $Time_{6-12M}$(right column of Table 2), that were statistically significantly different at $p<0.05$, between the two different EDSS groups (G_1 vs G_2) investigated in this study. Feature groups with the higher number of statistically different features were the RUNL, NGTDM, $SGLDM_m$, FDTA and $SGLDM_r$. Figure 4 displays box plots for the median (IQR) for a selection of texture features from Table 2, that at year 10, exhibited statistically significant differences between the two groups (G_1 vs G_2), for $Time_{0M}$ (left panel) and $Time_{6-12M}$ (right panel), for all subjects examined in this study (G_1: EDSS$\leq$3.5, full line plots, G_2: EDSS$>$3.5, doted lines plots).

B. AM-FM ANALYSIS

We present high-scale AM-FM features for a G_1 lesion (EDSS=1.5) and a G_2 lesion (EDSS=9) in Fig. 5 at $Time_{6-12M}$. From the plots in Fig. 5 the high-scale IA image is much darker for G_2 than for G_1. Similarly, the high-scale IF magnitude for G_2 clearly contains much more lower values

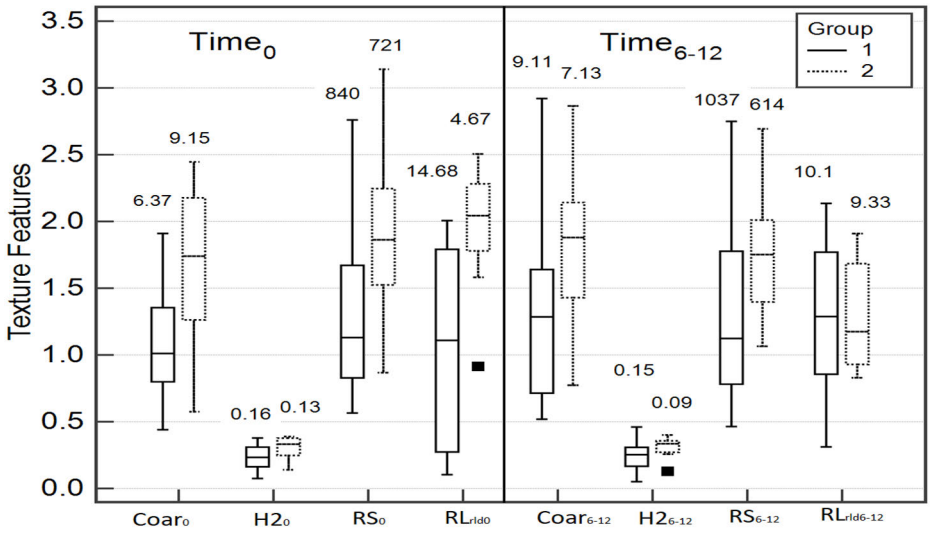

FIGURE 4. Box plots for texture features extracted from lesions at $Time_{0M}$ and $Time_{6-12M}$, for year 10: The texture futures Coarseness (Coar), H_2, Radial Sum (RS) and Run length distribution (RL_{RLD}) for $Time_{0M}$ (left panel) and $Time_{6-12M}$ (right panel), for the two different groups investigated in this study (G_1: Full line plots, G_2: Doted line plots).

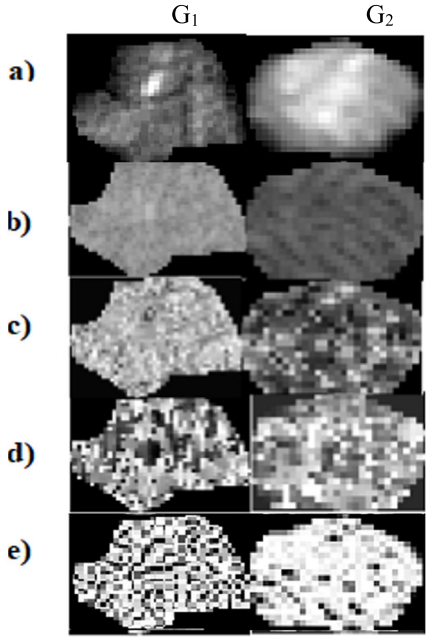

FIGURE 5. a) MS brain lesion (37pix-by-45pix) from a subject at G_1 (EDSS=1.5) at $Time_{6-12M}$ and a lesion (21pix-by-13pix) from a subject at G_2 (EDSS=9) in the left and right columns respectively (measured in $Time_{10Y}$). b) HIA, c) high |IF|, d) high angle IF, and e) high scale cos φ_n respectively.

than for G_1. The corresponding CDF plots for the two lesions are shown in Fig. 6. In Fig. 6, the lower IA and IF magnitude components result in early rises of the CDF plots for G_2 as compared to the CDF plots for G_1. The CDFs for the high IF magnitude exhibit the most significant differences between the two groups.

In Fig. 7, we show plots of G_1 vs G_2 median CDF as well as their corresponding shaded (IQR) values at $Time_{6-12M}$ based on the same AM-FM features presented in Fig. 6 using 14 bins. As before, there is a significant difference in the high-scale IF magnitude between the two groups.

Table 3 illustrates the AM-FM features median (IQR) values for the High-IF CDF component bins, extracted from the brain MS lesions at $Time_{0M}$ (left column) and $Time_{6-12M}$ months (right column), that were statistically significantly different between the two different groups (G_1/G_2) investigated in this study at year 10. It is shown that for the features at $Time_{0M}$ a better separation between the two different groups may be achieved, when using the High-IF CDF for bins 2 to 5 and the High-IF Angle CDF for bins 2 to 5. For the features at $Time_{6-12M}$a better separation between the two different groups may be achieved when using the HIF CDF for bins 2 to 9 and the HIF Angle CDF for bins 5 and 6.

C. CLASSIFICATION ANALYSIS

Table 4 tabulates the texture, AM-FM and MS lesion image classification evaluation results for the 10 different models investigated in this study. As shown, the deep learning classifier 4j, could achieve %CC of up to 87% when using Model 3, i.e., when combining both texture and AM-FM features together. When using the K-star by using all the information taken from the lesion images, the %CC shows considerable improvement. Model 10, which uses information from texture, AM-FM features and the lesion images could achieve a %CC of 94%.

IV. DISCUSSION

The main objective of the study was to determine whether the EDSS score could be used to assess the evolution of disease in MS patients to predict future disability by utilizing texture and AM-FM feature sets that were derived from

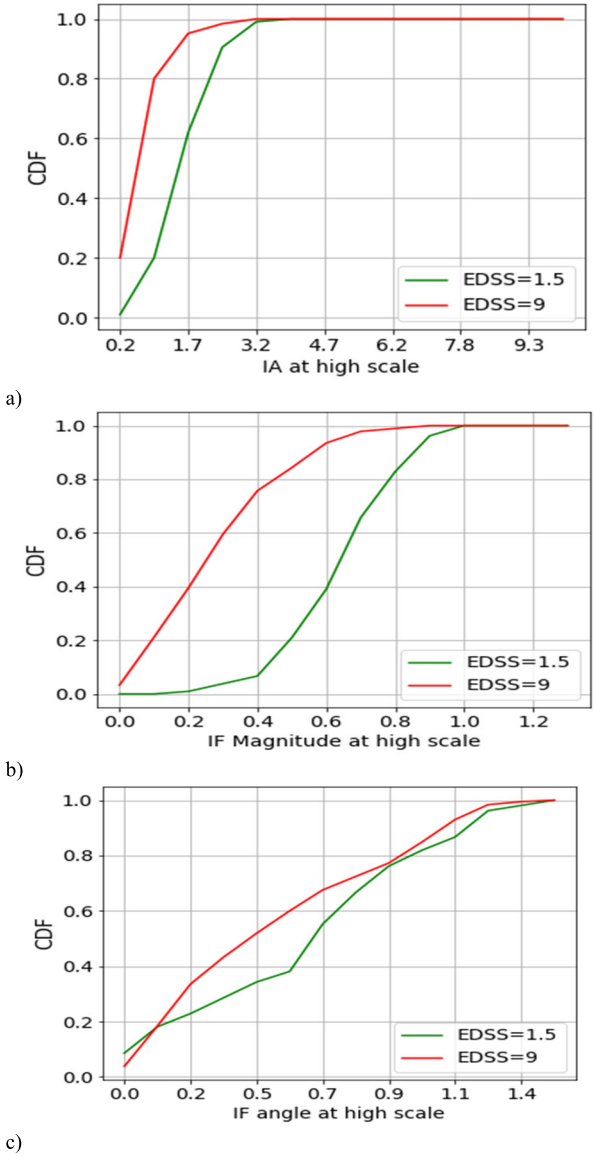

FIGURE 6. CDF plots computed from: a) HIA, b) high |IF|, and c) high angle IF respectively between a subject at G_1 (EDSS=1.5, green line) and a subject at G_2 (EDSS=9, red line) at $Time_{6-12M}$.

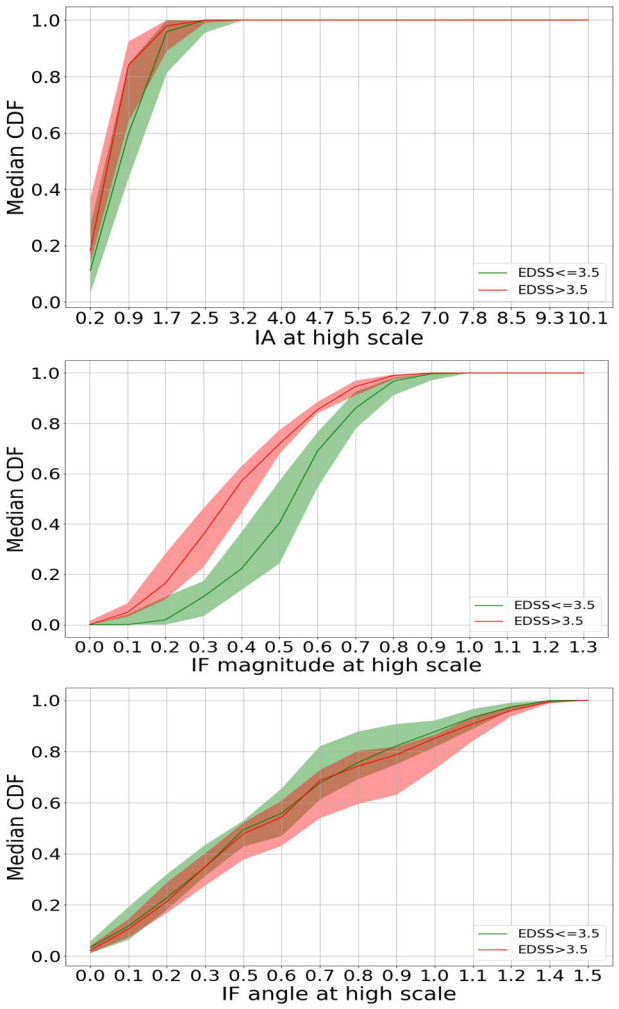

FIGURE 7. CDF Plots of the resulting median and shaded (IQR) in green for G_1 subjects (EDSS≤3.5) and in red for G_2 subjects (EDSS>3.5) at $Time_{6-12M}$ for the AM-FM features: a) HIA, b) high |IF| and c) high angle IF.

MRI MS detectable lesions. This will aid in decision making for personalized treatment and disease evolution prediction. We anticipate that we may thus be able to associate texture features with the progression of the MS disease. Since the use of quantitative MRI analysis as a surrogate outcome is also used as a surrogate measure in clinical trials, we hypothesize that there is a close relationship between the change in the extracted features and the clinical status and the rate of development of disability. We analyzed images acquired at the initial ($Time_{0M}$ and $Time_{6-12M}$) stages of the disease and we correlated texture and AM-FM findings with disability assessment scales. We interrelated therefore the EDSS scores with texture features.

Analysis was carried out in this study, using the sample of 38 subjects with CIS, also used in other earlier studies performed by our group [9], [10]. As also illustrated in Fig. 3 the subjects were separated into non-overlapping groups (G_1 (full line plots) vs G_2 (dotted line plots)), in $Time_{2Y}$, $Time_{5Y}$ and $Time_{10Y}$ based on their $EDSS_{10Y}$ score. We based our analysis on the manually segmented MS lesions from the acquired MRI scans at $Time_{0M}$ and $Time_{6-12M}$ and used the EDSS scores taken 10 years after the initial MRI examination to find features that will be able to predict the outcome of the MS disease.

The main findings of our study can be summarized as follows: (i) We found several statistically significant texture (see Table 2) and AM-FM (see Table 3) features that may be used to distinguish between the two different groups investigated in this study (G_1 vs G_2) at year 10. These features may thus be used to follow up MS disease evolution. (ii) MS lesion texture AM-FM and image classification models were used to predict the EDSS score (EDSS≤3.5 vs 3.5<EDSS≤10.0) (see also Table 4). (iii) It was found the HIF CDF AM-FM component may be used to best separate the two groups

TABLE 5. Selected studies predicting ms disease evolution.

Author	Year	CIS	G_1 vs G_2 EDSS	Year EDSS	Lesion Features	Classifier	ACC
Theocharakis [46]	2009	29	≤3.5 vs >4.0	3	Contrast, Homogeneity Roughness	PNN	89%
Loizou [10]	2011	38	≤2.0 vs >2.0	2	IA, |IF|, IF angle	SVM	86%
Gumberz [53]	2016	82	≤1.5 vs ≧5.0	1	Volume changes	CNNs	81%
Zhang [43]	2019	84	≤2.5 vs 3.0-6.5	3	Shape, Brightness, Volume	Random Forest	85%
Tousignant [48]	2019	465	<5.5 vs > 6.0	1	Lesion ROIs fed to CNN	CNN	71%
Narayana [56]	2019	1088	< 5.5 vs ≧5.5	1	Lesion ROIs fed to CNN	CNN	84%
This Study	2023	38	≤3.5 vs >3.5	10	Texture & AM-FM Features & Lesion ROIs	CNN	94%

N: Number of subjects investigated, CIS: Clinical isolated syndrome, G_1, G_2: EDSS Patient Groups, Year: Year EDSS was assessed, DL: Deep-Learning, PNN: Probabilistic neural network, CNN: Convolutional Neural Networks, SVM: Support vector machines, IA: Instantaneous amplitude, IF: Instantaneous frequency, AM-FM: Amplitude Modulation-Frequency Modulation, ACC: Accuracy of MS disease prediction.

(G_1 vs G_2) investigated in this study (see also Fig. 6, Fig. 7 and Table 3). (iv) The best classification results were obtained when using the texture and AM-FM features extracted from the MS lesions that were statistical significantly different between the two groups (G_1 vs G_2) as well as features lesion images, using the K-Star Beta (B 20-Ma) classifier from the Weka image classification toolbox [40]. The classification accuracy for predicting the two classes of the EDSS score was %CC=91% for $Time_{0M}$ and %CC=94% for $Time_{0M}$ + $Time_{6-12M}$ feature sets respectively when using texture, AM-FM as well as MS lesion images (see Table 4).

A comparative analysis table tabulating selected MS disease evolution studies is given in Table 5. This table summarizes the prediction of EDSS score into two different groups (G_1 vs G_2) at years one to three based on texture and AM-FM feature sets and images of the ROI lesions. Based on this table, the necessity and importance of this study is clearly motivated as to the best of our knowledge, there is no other study investigating MS disease prediction at year 10.

A. GENERAL DISCUSSION

A large number of studies were reported in the literature in order to establish a relationship between the various gray levels and texture features derived from brain scans [8], [9], [10], [13], [14], [15], [16], [17], [18], [19], [25], [29]. It was also documented that texture features (shown in Table 2 and Table 3), might encode meaningful interpretations regarding the clinical context of MS lesions and NAWM [30]. It was furthermore shown in [17], that histograms can characterize changes between MS lesions and NAWM. Table 5 tabulates selected studies proposed in the literature for the prediction of the MS disease evolution. An oblique random forest classifier was used based on the shape parameters of the lesions, where the conversion of CIS to MS was accurately predicted in 79% of the subjects (64 out of 84 subjects). In [44], it was also shown that the fractal dimension features extracted from the brain MS lesions in 146 subjects may to some extent identify patients with brain damage at a higher risk of disability progression in short to mid-term. Linear mixed models and the cumulative probability were used for the statistical analysis. In all of the above studies texture and shape analysis was performed on MR images of MS subjects and a combined set of texture features were investigated in order to better discriminate tissue between MS lesions, NAWM and NWM. Classification analysis was also performed for the differentiation of malignant tissue masses in MRI images of the brain [45]. In another study [46], a pattern recognition system was used for the discrimination of clinical definitive MS from clinically definitive microangiopathy lesions based on computer-assisted texture analysis of MRI images.

A related field of texture analysis is the AM-FM analysis [10], of images such as the one presented in the current study, where AM-FM characteristics are extracted from images [27].

AM-FM models have also been used in a variety of applications including image reconstruction [27], image retrieval [27], video processing such as motion estimation and video analysis [27], and enhancement and classification of medical images [47]. In [10], AM-FM analysis was performed on the normal tissue, NAWM, and lesions, on 38 MR images with a CIS of MS. MRI detectable brain lesions were scanned twice with an interval of 6-12 months. The results indicate that high-frequency IA can be used to differentiate between early and advanced cases of MS lesions (see also Table 5).

In another study [47], a multiscale spectral approach was introduced for the early disease detection in malignant brain tumor MRI and lung computed tomographic images. It was based on a dyadic filter bank extended to six scales for simultaneous modulation of the frequency and amplitude signal of the medical image. The modulated signal strength was used for enhancing the contrast of the image as a pre-processing step. AM-FM features were extracted from the 32 bin spectral image histogram and used with an SVM classifier for the early detection of the abnormalities.

The gray scale median value is an index that intuitively shows the brightness of each ROI. It was shown in [9] that MS lesions are brighter than NWM and that MS regions had higher contrast values than NWM regions. IDM is related to lesions homogeneity [9], [30]. These findings agree with observations by Mathias et al. [25] regarding MS lesions. The latter were found with increased entropy and decreased angular second moment, implying that MS lesion texture was rough and of low homogeneity. This loss of homogeneity in MS may be attributed to a number of processes such as gliosis, inflammation, demyelination and changes in water content that may disrupt MR signal intensity uniformity [25].

Tozer et al. [16], estimated several texture features that were significantly differed between subjects with MS and healthy subjects. Texture feature abnormalities in MS suggested there might be tissue damage beyond classic white matter lesions and that these features show potential for quantifying the severity of demyelination.

A deep learning convolutional neural network for the prediction of future subject disability progression (one year from baseline), based on multi-modal brain MRI MS images at baseline, was applied on 465 patients with MS in [48]. Using the baseline EDSS, it was shown that the model could predict future disease progression, measured by a sustained increase in the EDSS score over time. More specifically, if the baseline EDSS=0 then an increase of 1.5 or more in EDSS could be predicted in 12 weeks or more. The model was trained on two proprietary, multi-scanner, multicentre, clinical trial datasets of patients with relapsing-remitting MS by incorporating the clinician's assessment. The AUC was 0.701±0.027.

In [49], changes in MS lesions and relapses were followed up for 2 years in 560 MS patients. It was revealed that the combination of lesion changes and relapses may be used as a combined measure to predict disability progression. Likewise, in [50], MS disease severity prediction (EDSS worsening), was correlated with reduced brain volume and increased clinical relapses in 3635 MS patients. Furthermore, in [51] it was documented that gray matter atrophy was a common denominator for disability in Japanese and White patients. Additional contributory factors for future disability included T2W-lesion volume in Japanese patients and white matter atrophy in White patients. Similar findings were also reported by Luchetti et al. [52], where 182 MS subjects were investigated. It was shown that, patients that had a more severe disease course showed a higher proportion of mixed active/inactive lesions and a higher lesion load ($p = 2e{-}04$) at the time of death. Patients with a progressive disease course show a higher lesion load, and a lower proportion of demyelinated lesions ($p = 0.03$) compared to patients with a relapsing disease course.

Gumbez et al. [53], investigated the predictive value of MRI classification criteria in high/low atrophy and inflammation groups based on two consecutive routines MRI scans for disability progression in 82 MS subjects based on their EDSS (EDSS $\leq$1.5 and EDSS5.0) scores. Lower baseline EDSS and higher grey matter atrophy were the best predictors ($\rho = 0.54$) for EDSS progression, and the accuracy was equal to 0.81. Likewise, in [54], it was shown that a dissociation may occur between physical disability and cerebral lesion volume in either direction in patients with MS. Type of MS and brain lesions may help to bridge this dissociation. In [55], brain atrophy was measured in 164 healthy, 1514 MS and 1137 CIS subjects and its association with disability progression, was followed in a clinical routine over 5 years. All brain volume measures differentiated MS and healthy subjects and were associated with disability, but the lateral ventricle volume assessment was the most feasible. Furthermore, in [56] a deep learning neural network was used to predict the development of new MS lesions in 1008 subjects. The AUC which was achieved was 0.82±0.02. Cree et al. [57], characterized the long-term disease course of the MS disease in 517 MS subjects. They showed that clinical and radiologic features at baseline and the change over 2 years had predictive value for long-term MS disability. At a median time of 16.8 years after disease onset, 10.7% of patients reached an EDSS6, and 18.1% evolved from relapsing MS to secondary progressive MS. In [58], machine learning was used to identify four different MS groups (N=6322 MS subjects) with similar features using multidimensional data based on their clinical evolution (ACC=63%). MS lesions were defined into four different MS subtypes (cortex-led, normal-appearing white matter-led, and lesion-led). It was found that MRI-based subtypes can successfully predict MS disability progression and response to treatment and may be used to define groups of patients in interventional trials.

Finally, in [59] an automated method for counting pathologically distinct lesions using images obtained at a single time point, allowing for an accurate reconstruction of the natural history of lesion formation without longitudinal data was introduced. Lesion count was found to be significantly associated with EDSS.

B. LIMITATIONS

Detailed discussion of the limitations of the present study has also been discussed in other studies performed by our group [9], [10].

MRI images may also suffer from artifacts of different origins, such as image thermal noise, image background non-uniformity from magnetic field inhomogeneities, and no standardization of image gray-scale intensity. High image quality and minimization of these artifacts are important for performing quantitative analysis. The intensity normalization method firstly proposed in [28] and then later applied in [24] was used in this study. The proposed normalization method allows the scanner sensitivity variations and variations due to repeatability studies to be largely corrected and thereby facilitating meaningful comparisons between MRI data sets obtained at different times and/or different subjects. By normalizing the histogram of the whole brain, we introduced an automatic procedure with little sensitivity to pathological or morphological changes between the different image data sets. The method does not depend on knowledge of the scanner calibration and thus can be used on retrospective data. However, for the generalizability of the proposed methods and classification models, it is essential that further testing be conducted on a heterogeneous data set.

Furthermore, the 2-D images used for the analysis in this study had a slice thickness of 5 mm and this could introduce partial averaging that could compromise the quality of texture, AM-FM analysis, and classification. Higher-spatial-resolution images that are typically acquired in the three-dimensional mode would have been preferable [60]. Another limitation of this study was that it was based on conventional MRI sequences. Advanced MRI sequences such

as diffusion-weighted imaging, magnetization transfer ratio imaging, and myelin fraction mapping could be used. It might be possible that the inclusion of these additional sequences would increase the accuracy of identification of enhancing lesions as it was shown in [61], [62], and [63]. It is also anticipated that the inclusion of other MRI sequences may further improve the deep learning and classification process.

Finally, the dataset used in this study might be considered small, and it is therefore highly recommended to further validate the present results on a dataset with a larger number of subjects as well as on additional datasets collected from different medical centers. The evaluation of the findings of this study on datasets with a larger number of subjects will result in more stable model parameter estimates and more robust evaluation of model training and testing. Additionally, it will aid in the computation of additional features that may provide information for better and earlier differentiation between normal tissue and MS lesions for an accurate disease prognosis and follow up.

C. FUTURE WORK

In a future study we also intent to investigate how other clinical and paraclinical parameters like age, gender, [64], intrathecal synthesis of oligoclonal bands [65] or inflammatory cerebrospinal fluid [66] can be used to further improve prediction accuracy. Moreover, the disease course in MS subjects is individual. Therefore, rather than only predicting conversion in CIS subjects, it also appears promising to predict different disease courses and identify subjects who are likely to profit most from early treatment, considering different patterns of disease activity in MS subjects. Furthermore, exploring ways to interpret the predictions of the model and identify which regions of the brain contributed to the final decisions could help reveal new MS biomarkers, guiding the way of future research and furthering our understanding of the disease. Further future directions include improvements in the measurement and preprocessing of the image by applying image normalization, and validation of the results in a larger number of subjects. MRI texture, AM-FM and classification analyses of lesions in MS can also help in specifying the types of MS (CIS, primary progressive MS, progressive-relapsing MS, relapsing-remitting MS), secondary progressive MS based on the differences in analyses between the groups.

In addition, ongoing work covers the extraction of rules based on lesion texture features to provide explainability functionality about the progression of the disease [67]. Moreover, work in progress by our group includes the integration of the above with a semi-automated lesion segmentation system combined with 3D brain MRI reconstruction towards providing an integrated lesion visualization tool to the neurologist and neuro radiologist.

REFERENCES

[1] S. Vukusic and C. Confavreux, "Natural history of multiple sclerosis: Risk factors and prognostic indicators," *Current Opinion Neurol.*, vol. 20, no. 3, pp. 269–274, Jun. 2007.

[2] M. A. Rocca, M. P. Amato, N. De Stefano, C. Enzinger, J. J. Geurts, and I.-K. Penner, "Clinical and imaging assessment of cognitive dysfunction in multiple sclerosis," *Lancet Neurol.*, vol. 14, no. 3, pp. 302–317, 2015.

[3] M. Filippi, D. W. Paty, L. Kappos, F. Barkhof, D. A. S. Compston, A. J. Thompson, G. J. Zhao, C. M. Wiles, W. I. McDonald, and D. H. Miller, "Correlations between changes in disability and T2-weighted brain MRI activity in multiple sclerosis: A follow-up study," *Neurology*, vol. 45, no. 2, pp. 255–260, Feb. 1995.

[4] W. I. McDonald, A. Compston, G. Edan, D. Goodkin, H.-P. Hartung, F. D. Lublin, H. F. McFarland, D. W. Paty, C. H. Polman, S. C. Reingold, M. Sandberg-Wollheim, W. Sibley, A. Thompson, S. Van Den Noort, B. Y. Weinshenker, and J. S. Wolinsky, "Recommended diagnostic criteria for multiple sclerosis: Guidelines from the international panel on the diagnosis of multiple sclerosis," *Ann. Neurol.*, vol. 50, no. 1, pp. 121–127, 2001.

[5] C. H. Polman, "Diagnostic criteria for multiple sclerosis: 2010 revisions to the McDonald criteria," *Ann. Neurol.*, vol. 69, no. 2, pp. 292–302, 2011.

[6] A. J. Thompson et al., "Diagnosis of multiple sclerosis: 2017 revisions of the McDonald criteria," *Lancet Neurol.*, vol. 17, no. 2, pp. 162–173, 2018.

[7] A. J. Thompson and J. C. Hobart, "Multiple sclerosis: Assessment of disability and disability scales," *J. Neurol.*, vol. 245, no. 4, pp. 189–196, Apr. 1998.

[8] A. Kassner and R. E. Thornhill, "Texture analysis: A review of neurologic MR imaging applications," *Amer. J. Neuroradiol.*, vol. 31, pp. 809–816, May 2010.

[9] C. P. Loizou, S. Petroudi, I. Seimenis, M. Pantziaris, and C. S. Pattichis, "Quantitative texture analysis of brain white matter lesions derived from T2-weighted MR images in MS patients with clinically isolated syndrome," *J. Neuroradiology*, vol. 42, no. 2, pp. 99–114, Apr. 2015.

[10] C. P. Loizou, V. Murray, M. S. Pattichis, I. Seimenis, M. Pantziaris, and C. S. Pattichis, "Multiscale amplitude-modulation frequency-modulation (AM–FM) texture analysis of multiple sclerosis in brain MRI images," *IEEE Trans. Inf. Technol. Biomed.*, vol. 15, no. 1, pp. 119–129, Jan. 2011.

[11] M. Filippi, P. Preziosa, B. L. Banwell, F. Barkhof, O. Ciccarelli, N. De Stefano, J. J. G. Geurts, F. Paul, D. S. Reich, A. T. Toosy, A. Traboulsee, M. P. Wattjes, T. A. Yousry, A. Gass, C. Lubetzki, B. G. Weinshenker, and M. A. Rocca, "Assessment of lesions on magnetic resonance imaging in multiple sclerosis: Practical guidelines," *Brain*, vol. 142, no. 7, pp. 1858–1875, 2019.

[12] L. K. Fisniku, P. A. Brex, D. R. Altmann, K. A. Miszkiel, C. E. Benton, R. Lanyon, A. J. Thompson, and D. H. Miller, "Disability and T2 MRI lesions: A 20-year follow-up of patients with relapse onset of multiple sclerosis," *Brain*, vol. 131, no. 3, pp. 808–817, Feb. 2008.

[13] P. A. Brex, O. Ciccarelli, J. I. O'Riordan, M. Sailer, A. J. Thompson, and D. H. Miller, "A longitudinal study of abnormalities on MRI and disability from multiple sclerosis," *New England J. Med.*, vol. 346, no. 3, pp. 158–164, Jan. 2002.

[14] I. Dimitrov, S. Affiliate. Department of NursingMedical UniversityVarna, R. Georgiev, A. Kaprelyan, N. Usheva, M. Grudkova, K. Drenska, and B. Ivanov, "Brain and lesion volumes correlate with EDSS in relapsing remitting multiple sclerosis," *J. IMAB Annu. Proc. Sci. Papers*, vol. 21, no. 4, pp. 1015–1018, Dec. 2015.

[15] Y. Shao, Z. Chen, S. Ming, Q. Ye, Z. Shu, C. Gong, P. Pang, and X. Gong, "Predicting the development of normal-appearing white matter with radiomics in the aging brain: A longitudinal clinical study," *Frontiers Aging Neurosci.*, vol. 10, pp. 1–10, Nov. 2018.

[16] D. J. Tozer, E. Zeestraten, A. J. Lawrence, T. R. Barrick, and H. S. Markus, "Texture analysis of T1-weighted and fluid-attenuated inversion recovery images detects abnormalities that correlate with cognitive decline in small vessel disease," *Stroke*, vol. 49, no. 7, pp. 1656–1661, Jul. 2018.

[17] V. Tomassini, F. Fanelli, L. Prosperini, R. Cerqua, P. Cavalla, and C. Pozzilli, "Predicting the profile of increasing disability in multiple sclerosis," *Multiple Sclerosis J.*, vol. 25, no. 9, pp. 1306–1315, Aug. 2019.

[18] C. Tozlu, D. Sappey-Marinier, G. Kocevar, F. Cotton, S. Vukusic, F. Durand-Dubief, and D. Maucort-Boulch, "Modeling individual disability evolution in multiple sclerosis patients based on longitudinal multimodal imaging and clinical data," *bioRxiv*, pp. 1–22, Aug. 2019, doi: 10.1101/733295.

[19] L. C. V. Harrison, M. Raunio, K. K. Holli, T. Luukkaala, S. Savio, I. Elovaara, S. Soimakallio, H. J. Eskola, and P. Dastidar, "MRI texture analysis in multiple sclerosis: Toward a clinical analysis protocol," *Academic Radiol.*, vol. 17, no. 6, pp. 696–707, Jun. 2010.

[20] K.-O. Lövblad, N. Anzalone, A. Dörfler, M. Essig, B. Hurwitz, L. Kappos, S.-K. Lee, and M. Filippi, "MR imaging in multiple sclerosis: Review and recommendations for current practice," *Amer. J. Neuroradiology*, vol. 31, no. 6, pp. 983–989, Jun. 2010.

[21] J. Dehmeshki, G. J. Barker, and P. S. Tofts, "Classification of disease subgroup and correlation with disease severity using magnetic resonance imaging whole-brain histograms: Application to magnetization transfer ratios and multiple sclerosis," *IEEE Trans. Med. Imag.*, vol. 21, no. 4, pp. 320–331, Apr. 2002.

[22] S. Herlidou-Meme, J. M. Constans, B. Carsin, D. Olivie, P. A. Eliat, L. Nadal-Desbarats, C. Gondry, E. L. Rumeur, and I. Idy-Peretti, "MRI texture analysis on texture test objects, normal brain and intracranial tumors," *Magn. Reson. Imag.*, vol. 21, no. 9, pp. 989–993, 2003.

[23] D. S. Meier and C. R. G. Guttmann, "Time-series analysis of MRI intensity patterns in multiple sclerosis," *NeuroImage*, vol. 20, no. 2, pp. 1193–1209, Oct. 2003.

[24] G. Collewet, M. Strzelecki, and F. Mariette, "Influence of MRI acquisition protocols and image intensity normalization methods on texture classification," *Magn. Reson. Imag.*, vol. 22, no. 1, pp. 81–91, Jan. 2004.

[25] J. M. Mathias, P. S. Tofts, and N. A. Losseff, "Texture analysis of spinal cord pathology in multiple sclerosis," *Magn. Reson. Med.*, vol. 42, no. 5, pp. 929–935, Nov. 1999.

[26] J. Zhang, L. Tong, L. Wang, and N. Li, "Texture analysis of multiple sclerosis: A comparative study," *Magn. Reson. Imag.*, vol. 26, no. 8, pp. 1160–1166, Oct. 2008.

[27] K. P. Constantinou, I. P. Constantinou, C. S. Pattichis, and M. S. Pattichis, "Medical image analysis using AM-FM models and methods," *IEEE Rev. Biomed. Eng.*, vol. 14, pp. 270–289, 2021.

[28] M. Nixon and A. Aguado, *Feature Extraction & Image Processing*, Newness, 2002.

[29] D. J. Tozer, G. Marongiu, J. K. Swanton, A. J. Thompson, and D. H. Miller, "Texture analysis of magnetization transfer maps from patients with clinically isolated syndrome and multiple sclerosis," *J. Magn. Reson. Imag.*, vol. 30, no. 3, pp. 506–513, Sep. 2009.

[30] Y. Zhang, H. Zhu, J. R. Mitchell, F. Costello, and L. M. Metz, "T2 MRI texture analysis is a sensitive measure of tissue injury and recovery resulting from acute inflammatory lesions in multiple sclerosis," *NeuroImage*, vol. 47, no. 1, pp. 107–111, Aug. 2009.

[31] R. M. Haralick, K. Shanmugam, and H. DinsteinI, "Texture features for image classification," *IEEE Trans. Syst. Man Cybern.*, vol. SMC-3, no. 6, pp. 610–621, Nov. 1973.

[32] J. S. Weszka, C. R. Dyer, and A. Rosenfeld, "A comparative study of texture measures for terrain classification," *IEEE Trans. Syst., Man, Cybern.*, vol. SMC-6, no. 4, pp. 269–285, Apr. 1976.

[33] M. Amadasun and R. King, "Textural features corresponding to textural properties," *IEEE Trans. Syst., Man, Cybern.*, vol. 19, no. 5, pp. 1264–1274, Oct. 1989.

[34] C. M. Wu, Y. C. Chen, and K.-S. Hsieh, "Texture features for classification of ultrasonic liver images," *IEEE Trans. Med. Imag.*, vol. 11, no. 2, pp. 141–152, Jun. 1992.

[35] M. M. Galloway, "Texture analysis using gray level run lengths," *Comput. Graph. Image Process.*, vol. 4, no. 2, pp. 172–179, Jun. 1975.

[36] W. J. Conover, *Practical Nonparametric Statistics*, 3rd ed. New York, NY, USA: Wiley, 1999.

[37] D. G. Altman, *Practical Statistics for Medical Research*, London, U.K.: Chapman & Hall, 1991.

[38] University of Waikato. (2016). *Weka 3.8 Workbench-Waikato Environment for Knowledge Analysis*. [Online]. Available: http://www.cs.waikato.ac.nz/ml/index.html

[39] V. Vapnik, S. E. Golowich, and A. J. Smola, "Support vector method for function approximation, regression estimation and signal processing," in *Advances in Neural Information Processing Systems*, vol. 9. San Mateo, CA, USA: Morgan Kaufmann, 1997, pp. 281–287.

[40] S. Lang, F. Bravo-Marquez, C. Beckham, M. Hall, and E. Frank, "WekaDeeplearning4j: A deep learning package for Weka based on Deeplearning4j," *Knowl.-Based Syst.*, vol. 178, pp. 48–50, Aug. 2019.

[41] A. Larroza, D. Moratal, A. Paredes-Sánchez, E. Soria-Olivas, M. L. Chust, L. A. Arribas, and E. Arana, "Support vector machine classification of brain metastasis and radiation necrosis based on texture analysis in MRI," *J. Magn. Reson. Imag.*, vol. 42, no. 5, pp. 1362–1368, Nov. 2015.

[42] S. Tantisatirapong, N. P. Davies, D. Rodriguez, L. Abernethy, D. P. Auer, C. A. Clark, R. Grundy, T. Jaspan, D. Hargrave, L. MacPherson, M. O. Leach, G. S. Payne, B. L. Pizer, A. C. Peet, and T. N. Arvanitis, "Magnetic resonance texture analysis: Optimal feature selection in classifying child brain tumors," in *Proc. 13th Medit. Conf. Med. Biol. Engin. Comput. Medicon*. Spain: Springer, 2014, pp. 309–312.

[43] H. Zhang, H. Zhang, E. Alberts, V. Pongratz, M. Mühlau, C. Zimmer, B. Wiestler, and P. Eichinger, "Predicting conversion from clinically isolated syndrome to multiple sclerosis—An imaging-based machine learning approach," *NeuroImage, Clin.*, vol. 21, Jan. 2019, Art. no. 101593.

[44] E. Roura and G. Maclair, "Cortical fractal dimension predicts disability worsening in multiple sclerosis patients," *NeuroImage Clin.*, vol. 30, Jan. 2021, Art. no. 102653.

[45] M. E. Mayerhoefer, M. Breitenseher, G. Amann, and M. Dominkus, "Are signal intensity and homogeneity useful parameters for distinguishing between benign and malignant soft tissue masses on MR images?: Objective evaluation by means of texture analysis," *Magn. Reson. Imag.*, vol. 26, no. 9, pp. 1316–1322, Nov. 2008.

[46] P. Theocharakis, D. Glotsos, I. Kalatzis, S. Kostopoulos, P. Georgiadis, K. Sifaki, K. Tsakouridou, M. Malamas, G. Delibasis, D. Cavouras, and G. Nikiforidis, "Pattern recognition system for the discrimination of multiple sclerosis from cerebral microangiopathy lesions based on texture analysis of magnetic resonance images," *Magn. Reson. Imag.*, vol. 27, no. 3, pp. 417–422, Apr. 2009.

[47] A. Vidyarthi, "Multi-scale dyadic filter modulation based enhancement and classification of medical images," *Multimedia Tools Appl.*, vol. 79, nos. 37–38, pp. 28105–28129, Oct. 2020.

[48] A. Tousignant, P. Lematre, D. Precup, D. L. Arnold, and T. Arbel, "Prediction of disease progression in multiple sclerosis patients using deep learning analysis of MRI data," in *Proc. Int. Conf. Med. Imag. Deep Learn.*, vol. 102, 2019, pp. 483–492.

[49] M. P. Sormani, D. K. Li, P. Bruzzi, B. Stubinski, P. Cornelisse, S. Rocak, and N. De Stefano, "Combined MRI lesions and relapses as a surrogate for disability in multiple sclerosis," *Neurology*, vol. 77, no. 18, pp. 1684–1690, Nov. 2011.

[50] E.-W. Radue, F. Barkhof, L. Kappos, T. Sprenger, D. A. Haring, A. de Vera, P. von Rosenstiel, J. R. Bright, G. Francis, and J. A. Cohen, "Correlation between brain volume loss and clinical and MRI outcomes in multiple sclerosis," *Neurology*, vol. 84, no. 8, pp. 784–793, Feb. 2015.

[51] Y. Nakamura, L. Gaetano, T. Matsushita, A. Anna, T. Sprenger, E.-W. Radue, J. Wuerfel, L. Bauer, M. Amann, K. Shinoda, N. Isobe, R. Yamasaki, T. Saida, L. Kappos, and J.-I. Kira, "A comparison of brain magnetic resonance imaging lesions in multiple sclerosis by race with reference to disability progression," *J. Neuroinflammation*, vol. 15, no. 1, pp. 1–11, Dec. 2018.

[52] S. Luchetti, N. L. Fransen, C. G. van Eden, V. Ramaglia, M. Mason, and I. Huitinga, "Progressive multiple sclerosis patients show substantial lesion activity that correlates with clinical disease severity and sex: A retrospective autopsy cohort analysis," *Acta Neuropathologica*, vol. 135, no. 4, pp. 511–528, Apr. 2018.

[53] J. von Gumberz, M. Mahmoudi, K. Young, S. Schippling, R. Martin, C. Heesen, S. Siemonsen, and J.-P. Stellmann, "Short-term MRI measurements as predictors of EDSS progression in relapsing-remitting multiple sclerosis: Grey matter atrophy but not lesions are predictive in a real-life setting," *PeerJ*, vol. 4, p. e2442, Sep. 2016.

[54] B. C. Healy, G. J. Buckle, E. N. Ali, S. Egorova, F. Khalid, S. Tauhid, B. I. Glanz, T. Chitnis, C. R. G. Guttmann, H. L. Weiner, and R. Bakshi, "Characterizing clinical and MRI dissociation in patients with multiple sclerosis," *J. Neuroimaging*, vol. 27, no. 5, pp. 481–485, Sep. 2017.

[55] E. Ghione, N. Bergsland, M. G. Dwyer, J. Hagemeier, D. Jakimovski, I. Paunkoski, D. P. Ramasamy, D. Silva, E. Carl, D. Hojnacki, C. Kolb, B. Weinstock-Guttman, and R. Zivadinov, "Brain atrophy is associated with disability progression in patients with MS followed in a clinical routine," *Amer. J. Neuroradiology*, vol. 39, no. 12, pp. 2237–2242, Dec. 2018.

[56] P. A. Narayana, I. Coronado, S. J. Sujit, J. S. Wolinsky, F. D. Lublin, and R. E. Gabr, "Deep learning for predicting enhancing lesions in multiple sclerosis from noncontrast MRI," *Radiology*, vol. 294, no. 2, pp. 398–404, Feb. 2020.

[57] B. A. Gourraud, P. A. Oksenberg, J. R. Bevan, and E. Crabtree-Hartman, "Long-term evolution of multiple sclerosis disability in the treatment era," *Ann. Neurol.*, vol. 80, no. 4, pp. 499–510, 2016.

[58] A. Eshaghi, A. L. Young, P. A. Wijeratne, F. Prados, D. L. Arnold, S. Narayanan, C. R. G. Guttmann, F. Barkhof, D. C. Alexander, A. J. Thompson, D. Chard, and O. Ciccarelli, "Identifying multiple sclerosis subtypes using unsupervised machine learning and MRI data," *Nature Commun.*, vol. 12, no. 1, pp. 1–12, Apr. 2021.
[59] J. D. Dworkin, K. A. Linn, I. Oguz, G. M. Fleishman, R. Bakshi, and G. Nair, "An automated statistical technique for counting distinct multiple sclerosis lesions," *Amer. J. Neuroradiology*, vol. 39, no. 4, pp. 626–633, 2018.
[60] A. Crombé, M. Saranathan, A. Ruet, M. Durieux, E. de Roquefeuil, J. C. Ouallet, B. Brochet, V. Dousset, and T. Tourdias, "MS lesions are better detected with 3D T1 gradient-echo than with 2D T1 spin-echo gadolinium-enhanced imaging at 3T," *Amer. J. Neuroradiology*, vol. 36, no. 3, pp. 501–507, Mar. 2015.
[61] S. Rahimi, A. Azari, P. Ghaemmaghami, G. H. Meftahi, and G. P. Jahromi, "Detection of active plaques in multiple sclerosis using 3 and 12 directional diffusion-weighted imaging: Comparison with gadolinium-enhanced MR imaging," *J. Biomed. Phys. Eng.*, vol. 10, no. 6, pp. 737–744, Jun. 2018.
[62] C. Thaler, A. A. Kyselyova, T. D. Faizy, M. T. Nawka, S. Jespersen, B. Hansen, J.-P. Stellmann, C. Heesen, K. H. Stürner, M. Stark, J. Fiehler, M. Bester, and S. Gellißen, "Heterogeneity of multiple sclerosis lesions in fast diffusional kurtosis imaging," *PLoS ONE*, vol. 16, no. 2, Feb. 2021, Art. no. e0245844.
[63] J. Chen, C. Zhou, L. Zhu, X. Yan, Y. Wang, X. Chen, and S. Fang, "Magnetic resonance diffusion tensor imaging for occult lesion detection in multiple sclerosis," *Experim. Therapeutic Med.*, vol. 13, no. 1, pp. 91–96, Jan. 2017.
[64] V. Wottschel, D. C. Alexander, P. P. Kwok, D. T. Chard, M. L. Stromillo, N. De Stefano, A. J. Thompson, D. H. Miller, and O. Ciccarelli, "Predicting outcome in clinically isolated syndrome using machine learning," *NeuroImage: Clin.*, vol. 7, pp. 281–287, 2015.
[65] M. Tintore, A. Rovira, J. Rio, C. Tur, R. Pelayo, C. Nos, N. Tellez, H. Perkal, M. Comabella, J. Sastre-Garriga, and X. Montalban, "Do oligoclonal bands add information to MRI in first attacks of multiple sclerosis?" *Neurology*, vol. 70, no. 13, pp. 1079–1083, Mar. 2008.
[66] A. Ruet, G. Arrambide, B. Brochet, C. Auger, E. Simon, À. Rovira, X. Montalban, and M. Tintoré, "Early predictors of multiple sclerosis after a typical clinically isolated syndrome," *Multiple Sclerosis J.*, vol. 20, no. 13, pp. 1721–1726, Nov. 2014.
[67] A. Nicolaou, C. P. Loizou, M. Pantzaris, A. Kakas, and C. S. Pattichis, "Rule extraction in the assessment of brain MRI lesions in multiple sclerosis: Preliminary findings," in *Proc. 19th Int. Conf. Comp. Anal. Imag. Patterns*, Nicosia, Cyprus, N. Tsapatsoulis, Ed. vol. 13052, 2021, pp. 277–286.

CHRISTOS P. LOIZOU (Senior Member, IEEE) received the B.Sc., M.Sc., and Ph.D. degrees. He is currently an Adjunct Professor with the Department of Electrical Engineering, Computer Engineering and Informatics, Cyprus University of Technology, Cyprus. He is also an Associate Researcher with the Institute of Neurology and Genetics, Nicosia, Cyprus, and the Co-Founder and a member of the e-Health Laboratory, University of Cyprus. He has more than 25 years of experience in medical imaging and video analysis and processing. He has been involved in different projects in the above area funded by the Research Promotion Foundation of Cyprus and the EU and the National Institutes of Health (NIH-USA), with a total funding in the range of 12.5 million euros. He was a supervisor of a number of B.Sc. (83), M.Sc. (55), and Ph.D. (21) students in computer image, video analysis, and telemedicine. He has published 42 journal publications, 84 conference papers, five books, and 12 chapters in books in these areas (number of citations more than 3000, H-index: 28, i-10 index: 49, and RG score: 48.67). His research interests include medical imaging, video analysis and processing, motion analysis, signal processing, pattern recognition, voice stress signal analysis, biosignal analysis in ultrasound and magnetic resonance imaging, and video and computer applications in medicine. He has extensive experience in image/video pre-processing, despeckling, segmentation, and texture analysis. He serves as a reviewer for many IEEE Transactions journals and a Chair or a Co-Chair for many IEEE conferences.

KEVIN FOTSO (Member, IEEE) received the B.Sc. degree in biomedical engineering from the Illinois Institute of Technology, in 2012, and the M.S. degree in biomedical engineering from The University of New Mexico, in 2016, where he is currently pursuing the Ph.D. degree in biomedical engineering. He is a trained Cyber-Ambassador Facilitator and has some expertise in high-performance supercomputing. He is also a Project Lead the Way (PLTW)-certified Instructor. His research interests include multiple sclerosis lesion modeling and disability classification. He has served as a Reviewer for IEEE Journal of Biomedical and Health Informatics and a Grant Reviewer for The University of New Mexico Graduate and Professional Student Association.

ANTRIA NICOLAOU (Member, IEEE) received the B.Sc. degree in computer engineering with a minor in biomedical engineering from the University of Cyprus, in 2017, and the M.Sc. degree in molecular and applied physiology from the National and Kapodistrian University of Athens, in 2019. She is currently pursuing the Ph.D. degree with the Department of Computer Science, University of Cyprus, under the supervision of Prof. Constantinos S. Pattichis. Her research interest includes biomedical engineering.

MARIOS PANTZARIS received the M.D. degree in neurology from Aristotle University of Thessaloniki, Greece, in 1995. He received training in carotid duplex-Doppler ultrasonography from St. Mary's Hospital, London, in 1995. In 1999, he was a Visiting Doctor of acute stroke treatment at Massachusetts General Hospital, Harvard University, Boston. He is currently a Senior Consultant Neurologist and the Head of the Neurovascular Department, The Cyprus Institute of Neurology and Genetics, and an Associate Professor with the Cyprus School of Molecular Medicine. He is also the Head of the Multiple Sclerosis (MS) Clinic, where he is running research projects toward the etiology and therapy of MS. He has considerable experience in carotids-transcranial ultrasound, has participated in many research projects, and has several publications to his name.

MARIOS S. PATTICHIS (Senior Member, IEEE) received the B.Sc. degree (Hons.) in computer science, the B.A. degree (Hons.) in mathematics and a minor in electrical engineering, the M.S. degree in electrical engineering, and the Ph.D. degree in computer engineering from The University of Texas at Austin, in 1991, 1993, and 1998, respectively. He was a fellow of the Center for Collaborative Research and Community Engagement, College of Education, The University of New Mexico (UNM), from 2019 to 2020. He is currently a Professor with the Department of Electrical and Computer Engineering, UNM. At UNM, he is the Director of the Image and Video Processing and Communications Laboratory (ivPCL). His research interests include biomedical image analysis, image and video processing, video communications, audio processing, and

dynamically reconfigurable computer architectures. He held the 2019–2022 ECE Gardner Zemke Professorship for teaching. In 2022, he was elected as a fellow of the European Alliance of Medical and Biological Engineering and Science (EAMBES) for his contributions to biomedical image analysis. He was a recipient of the 2016 Lawton-Ellis and the 2004 Distinguished Teaching Awards from the Department of Electrical and Computer Engineering, UNM. For his development of the digital logic design labs at UNM, he was recognized by the Xilinx Corporation, in 2003, and by the UNM School of Engineering's Harrison Faculty Excellence Award, in 2006. He was the General Chair of the 2008 IEEE Southwest Symposium on Image Analysis and Interpretation (SSIAI), where he also served as the General Co-Chair, in 2020. He has served as a Senior Associate Editor for IEEE TRANSACTIONS ON IMAGE PROCESSING, a Senior Associate Editor for IEEE SIGNAL PROCESSING LETTERS, an Associate Editor for IEEE TRANSACTIONS ON IMAGE PROCESSING, *Pattern Recognition*, and IEEE TRANSACTIONS ON INDUSTRIAL INFORMATICS, and a Guest Associate Editor for Special Issues published in IEEE TRANSACTIONS ON INFORMATION TECHNOLOGY IN BIOMEDICINE, *Biomedical Signal Processing and Control*, and *Teachers College Record*, and a Pending Special Issue for IEEE JOURNAL OF BIOMEDICAL AND HEALTH INFORMATICS.

CONSTANTINOS S. PATTICHIS (Fellow, IEEE) is currently a Professor with the Department of Computer Science and the Director of the Biomedical Engineering Research Centre, University of Cyprus, and a Leader of HealthXR–Smart, Ubiquitous, and Participatory Technologies for Healthcare Innovation, CYENS—Centre of Excellence. He has 30 years of experience in eHealth and connected health, medical imaging, biosignal analysis, intelligent systems, and explainable AI, and more recently in mHealth interventions based on X Reality applications. He has been involved in numerous projects in these areas funded by EU and other bodies, with a total funding managed close to 15 million euros. He has published 130 journal publications, 236 conference papers, 30 chapters in books, 22 journal special issues, and 19 conference proceedings in his areas of interest. He is a fellow of IET, the International Academy of Medical and Biomedical Engineering (IAMBE), and the European Alliance for Medical and Biological Engineering and Science (EAMBES). He is an editor of three books.